# Microchannels With Manufacturing Roughness Levels

**S. A. Weaver**
e-mail: sweaver@sandia.gov

**M. D. Barringer**
e-mail: mbarringer@psu.edu

**K. A. Thole**
e-mail: kthole@psu.edu

Department of Mechanical and Nuclear Engineering,
The Pennsylvania State University,
University Park, PA 16802

*There are heat transfer advantages to reducing the size of channels used for internal cooling gas turbine components. As channel sizes decrease, however, there are concerns as to how manufacturing surface roughness may affect the channels' expected pressure drop and heat transfer. For microchannel size scales, in particular, there is relatively little data indicating the effect of manufacturing roughness levels. The focus of this paper is to describe the development and validation of a testing method for microchannels as well as to determine the effect of manufacturing roughness levels on these small channels. Convective heat transfer coefficients and friction factors were deduced based on measured flow conditions and known boundary conditions. It was shown that at an average roughness height of 6.1 $\mu$m, which corresponded to 2.2% of the channel height, heat transfer was augmented by 1.1–1.2, while the friction factor was augmented significantly more by 2.1–2.6 over a smooth channel.* [DOI: 10.1115/1.4002991]

## 1 Introduction

As turbine operating temperatures continue to rise, there is the ever present problem of cooling airfoil components. To accomplish this, cooling methods have morphed into a complex array of specialized internal and external schemes. A majority of cooling methods involve routing cool air from the compressor, through internal cooling channels and out through various film cooling holes around the blade surface. These cooling channels serve as a means to transfer heat from the airfoil surfaces to a cooling flow passing through the inside of the vanes and blades.

Internal cooling has evolved from simple smooth-walled channels to ones that include various types of turbulators that serve to increase the convective heat transfer coefficient and heat transfer surface area. Turbulators have been studied in detail over the years, and the most preferred cooling designs involve pedestals, ribs, and various surface roughening effects such as dimples. They serve to increase the turbulent mixing of the flow as it passes through the channel, thereby increasing the convective heat transfer coefficient along the wall surfaces.

There are many advantages from a cooling perspective to use microchannels to cool components, provided that the pressure to drive the flow through these channels is available. These microchannels approach the level where manufacturing (random) roughness and tolerances can play a key role in their heat transfer capabilities [1]. Average manufacturing roughness in common casting techniques can approach 1–10 $\mu$m [2] before polishing or finishing, and this seemly inconsequential inherent roughness can discernibly affect the microchannels' heat transfer and pressure drop.

This paper provides a summary of the findings of an experimental program focused on examining the heat transfer and pressure drop of microchannels. Accurately quantifying these two parameters will enable better prediction of the engine hardware thermal performance and life. The primary objective of this study was to develop a testing procedure capable of evaluating the heat transfer and pressure drop performance of several microchannels over a range of Reynolds numbers. The performance is reported in the form of an overall Nusselt number and friction factor for each manufacturing roughness level. While the results indicate little dependence of heat transfer and pressure drop augmentation upon Reynolds number, the range studied was in the fully turbulent regime in which compressibility effects were not present.

## 2 Relevant Past Studies

Microchannel cooling has only recently been studied in the gas turbine field. The main benefit from this method is that it provides minimal conductive thermal resistance between the cooling fluid and the external hot gases. However, microchannel cooling with surface roughness has been studied extensively for channel heights in the sub-500 $\mu$m range by the biomedical, electronics, and cryogenic cooling fields and in the large scale range (greater than 10 mm) by the heating, ventilating, and air conditioning (HVAC) and energy fields [3,4]. Very little data exist in the microchannel range between these two sizes, and yet the between range is the most applicable to the gas turbine fields.

The biomedical, electronics, and cryogenic cooling fields have focused on using single- and two-phase flows, liquid nitrogen, and other refrigerants having microchannel dimensions on the order of 20–500 $\mu$m [5,6]. The studies in these fields predominately focused on the laminar and transitional regimens and do not report data expansively into the fully turbulent regime.

Qi et al. [7] studied the effect of surface roughness on the cooling performance of liquid nitrogen in microchannels with diameters of 0.5–2 mm over a wider range of Reynolds numbers. Over a Reynolds number range of $1\times10^4$–$9\times10^4$, they found that roughness increased the heat transfer and pressure drop over a smooth channel, but the pressure drop augmentation was less at higher temperatures due to lower nitrogen viscosities.

In the sub-500 $\mu$m range, little data exist on gas cooled channels in the fully turbulent regime. Lorenzini et al. [8] studied nitrogen gas to cool circular microchannels with diameters of 25–508 $\mu$m. They found that at low Reynolds numbers in the laminar regime, their results accurately matched the literature results. However, when fully turbulent, the results deviated due to compressibility effects. Their reported data were in the fully turbulent regime but stopped at a Reynolds number of $1\times10^4$.

One of the first studies of microchannel heat transfer in the gas turbine field was performed by Marques and Kelly [9], where a pin fin microheat exchanger was developed having channels with a height of 0.5 mm that contained various pin turbulator geometries. The arrays had a height to diameter ratio of 1 and a staggered spacing to diameter ratio of 2.5. Over a Reynolds number range of $4\times10^3$–$2\times10^4$, the array augmented the heat transfer on the order of 4–5 and friction factor on the order of 15–20 over a smooth channel.

Contributed by the International Gas Turbine Institute (IGTI) of ASME for publication in the JOURNAL OF TURBOMACHINERY. Manuscript received July 1, 2010; final manuscript received July 8, 2010; published online April 21, 2011. Editor: David Wisler.

  

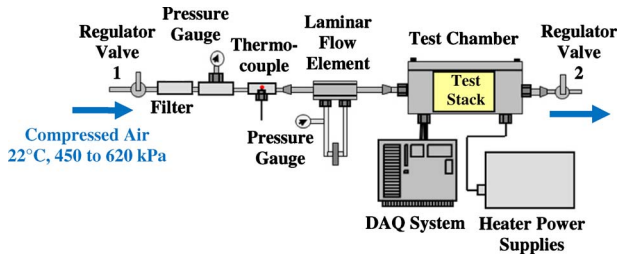


**Fig. 1 Schematic of the microchannel test apparatus designed in this study**

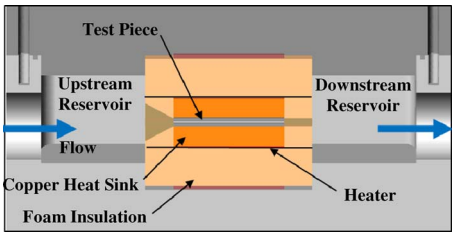


**Fig. 2 Axial view of the heat transfer test chamber and internal components**

Bunker et al. [10] studied various types of turbulators, including round and diamond pins and pins with various wall dimple configurations in small channels. He tested channel widths of 33 cm and heights of 5.08 mm, which gave an aspect ratio of 65:1 (W:H). Tests were conducted with round pedestal axial spacing to diameter ratios of 1.5 and height to diameter ratios of 0.2, which differs from usual array height to diameter ratios greater than 1. Bunker's findings indicated that the dense arrays augmented the heat transfer by approximately 2.25 times over a smooth channel. The arrays with pins and dimples performed better, augmenting the heat transfer by more than 3, but at a friction factor augmentation of up to 25.

Bunker [11] also studied the use of small pedestals in mesh-fed film cooling. The aim was to increase the film effectiveness downstream of a slot by placing small pedestal turbulators immediately upstream of the slot flow exit. The pedestal height to diameter ratio was 0.2, with slot blowing ratios of 0.1–0.7. The results were that the coolant stream did not blow off the wall, even at the higher blowing ratios where this would be expected. Cooling was augmented by 25–100% in the downstream section when compared with cooling with no turbulators.

As internal channels approach smaller and smaller dimensions, such as those being studied in this experiment, manufacturing tolerances can also play a role in the overall heat transfer performance of the channels. Bunker [1] performed a review on the effects of various tolerances on the cooling performance of channels that included film cooling, impingement cooling, internal cooling passages, and turbulated channels. The study concluded that channel geometry tolerances affected the heat transfer by 1%, but turbulator manufacturing tolerances affected the heat transfer even more by 2–7%.

This paper presents a method for discerning manufacturing roughness effects on heat transfer and pressure drop for microchannels that fall between the sub-500 $\mu$m and large scale (greater than 10 mm) ranges, which is relevant to gas turbine engines. The remainder of the paper presents the design and validation of the testing apparatus, followed by results of measured pressure drop and heat transfer for a number of test coupons.

## 3 Experimental Apparatus

A test stand and individual chambers were designed to test microchannel coupons and minimize the overall uncertainty of the heat transfer and pressure drop measurements. The overall apparatus is shown in Fig. 1. The primary components of the stand included a high pressure air supply line with a regulator valve, a primary test chamber, and a downstream exhaust line with a regulator valve. Compressed air was supplied to the test stand at 22°C and 450–620 kPa gauge, and the flow rate was measured using a laminar flow element located upstream of the test chamber. The high pressure air then passed into the test chamber and subsequently out through the second regulator valve, which was used to adjust the downstream pressure and flow rate through the chamber. Two test chambers were constructed: one for measuring heat transfer and one for measuring pressure drop. These two chambers were designed to be easily interchanged and to share the maximum common instruments between the two.

An axial cross-section of the heat transfer test chamber is shown in Fig. 2. The outer enclosure of the test chamber was fabricated from a hard plastic known as polyetheretherketone (PEEK) having 1.6 cm thick walls. This material was selected due to its low thermal conductivity, as shown in Table 1, high tensile strength, and good machining properties. A low thermally conductive material was necessary to minimize the heat loss from the test chamber to the surrounding atmosphere, while the high tensile strength was desirable due to the elevated operating air pressure within the test chamber. The PEEK test chamber contained a sandwich of pieces that included a stack of rigid foam insulation, copper heat sinks, electric circuit heaters, and the test coupon. Axially centering the stack gave identical reservoirs upstream and downstream to allow measurement of the inlet and outlet pressures and temperatures of the air.

The foam was rigid polyurethane and was selected due to its low thermal conductivity (as shown in Table 1) in combination with its other desirable characteristics including a wide temperature use range and high compressive strength.

Photographs of the test section construction are shown in Fig. 3. The foam was used as an insulator around the test coupon and copper heat sinks. The insulation reduced the heat loss from the heaters to approximately 2–4% for the range of Reynolds numbers tested. To ease the transition from the large upstream reservoir to the small coupon channel, a trapezoidal inlet was built into the foam insulation. Downstream of the coupon where the outlet air temperatures were measured, the channel had a constant cross-section.

The copper blocks were heated using two identical circuit heaters positioned between the copper and the surrounding foam in-

**Table 1 Test chamber thermal properties**

| Material | k (W/m K) |
|---|---|
| PEEK | 0.25 |
| Copper | 400 |
| Foam | 0.054 |
| Conductive paste | 2.31 |

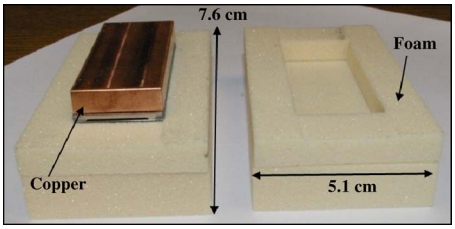


**Fig. 3 Photograph of the foam insulation used to surround the test coupon and heat sinks**

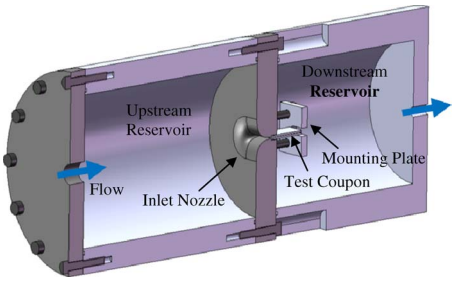


**Fig. 4 Axial view of the pressure drop test chamber and internal components**

sulation. The heaters were chosen for their ability to provide a constant heat flux boundary condition to the surface of the copper of up to 12.3 $W/cm^2$. Since copper has a very high thermal conductivity (as shown in Table 1), the constant heat flux being supplied by the heaters resulted in a copper heat sink that was nearly spatially uniform in temperature, as verified later in this study through numerical simulations. This uniform copper temperature was then the physical boundary condition for the test coupon.

To ensure all of the flow passed through the test coupon channel (and not around it through the foam stack), all upstream interfaces were sealed with a silicone sealant. In addition, all downstream edges were sealed using high vacuum grease.

The test chamber used to quantify pressure drop differed in the fact that there were no heaters or insulating materials needed, as shown in Fig. 4. This test chamber was manufactured to have an upstream chamber to decelerate the flow to measure a total upstream pressure, a nozzle inlet to the coupon, and a downstream chamber to measure total downstream pressure. The inlet nozzle was designed to reduce any entrance losses. The downstream reservoir provided the same benefit as in the heat transfer chamber, which was to provide a fixed back pressure to remain at low Mach numbers (less than 0.2) through the channel. The supply air pressure was kept at a constant pressure, and the downstream pressure was throttled with the regulator valve. The coupon was attached to the nozzle wall using a compression fitting with a notch cut into it as to not impede the exiting flow.

## 4 Instrumentation

For the heat transfer tests, the entire test apparatus, including the primary PEEK test chamber and the upstream delivery pipe, was instrumented to ensure measurement redundancies and minimize uncertainties. Figure 5 shows the locations in which temperature and pressure measurements were taken. All temperature measurements were performed using type-E thermocouples, with multiple temperature measurements made to verify an even temperature distribution across the pitch direction.

The copper heat sinks were each machined with six evenly spaced insertion holes that allowed the installation of thermocouples at the midplane of the heat sinks. Each insertion hole was filled with highly thermally conductive paste (as shown in Table 1). As with the copper blocks, temperature measurements were taken upstream and downstream of the coupon in the foam blocks. Six evenly spaced thermocouples were also positioned in the top and bottom foam pieces to calculate the amount of heat loss from the test chamber.

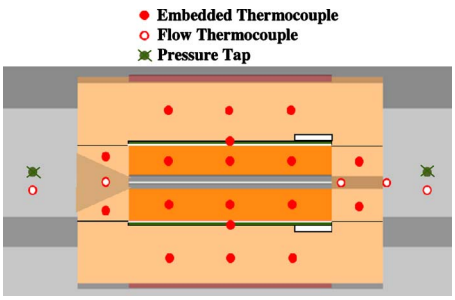


**Fig. 5 Drawing of the measurement locations within the test apparatus**

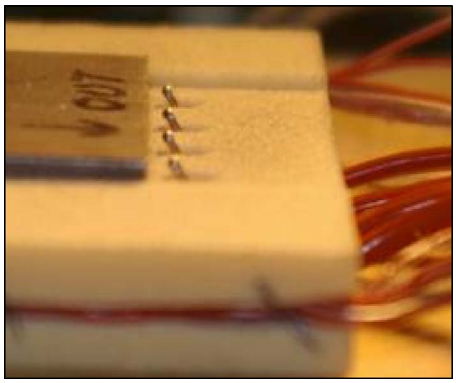

**Fig. 6 Photograph of thermocouples installed at channel exit**

Figure 6 shows examples of the thermocouples installed within the test stack that measured the coupon outlet air temperature. Four thermocouples were placed at the exit of the test coupon and four were placed at the exit of the foam. These two streamwise locations were used to provide two measurement points for accurately measuring the outlet temperature. The foam exit was used as the outlet location for calculating the overall heat transfer coefficient.

As for the pressure drop test chamber, pressure measurements were made in the upstream and downstream chambers and across the chambers. The individual pressures were used to calculate the air densities, while the differential measurement across the chambers provided an accurate measurement of the total pressure drop.

## 5 Microchannel Test Coupon

Four test coupons were manufactured for testing the effect of random manufacturing roughness in microchannels. They were fabricated out of a proprietary metal that had a high thermal conductivity relative to the insulating materials. To minimize the thermal resistance between the heaters and the copper blocks, as well as between the copper blocks and the test coupons, a thin layer (0.08 mm) of thermally conductive paste was applied across the outer surface of the test coupon (properties shown in Table 1).

To fabricate a microchannel with a specified surface roughness, the test coupons had to be manufactured in two separate parts and then attached, as seen in Fig. 7. The top and bottom pieces were fabricated using wire or plunge electric discharge machining that provided a specified surface roughness and then attached using a thermally conductive cold-weld on the streamwise sides of the pieces. Each test coupon had an internal channel width of 17.8 mm and a height of approximately 500 $\mu$m, which was measured using high accuracy pin gauges. The test coupons had an overall width of 2.5 cm and a length of 5.0 cm.

The parameters of the four test coupons tested are shown in Table 2, which includes the following: manufacturing method, average surface roughness ($R_a$), maximum surface roughness ($R_z$), and channel height (H). The average roughness was defined as the average of the differences between a roughness height and a roughness mean across the sample, while the maximum roughness range was the average of the ten largest differences between peaks and valleys [12]. The average and maximum surface roughnesses are described as a 95% confidence interval of the data measured on the top and bottom surfaces. The channel height is the height measured using the pin gauges plus $4R_a$, with an un-

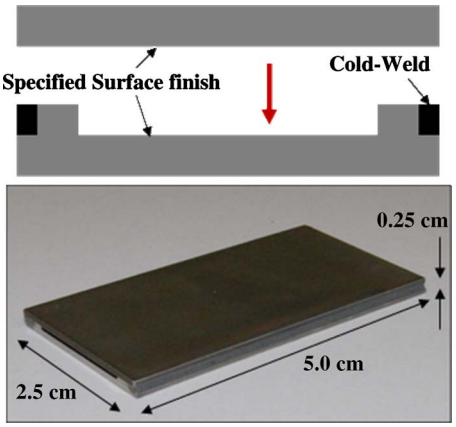


**Fig. 7 Diagram of test coupon assembly process and overall dimensions**

certainty calculated using the partial derivative method by Kline and McClintock [13]. Figure 8 shows a sample of a three-dimensional surface plot of coupon C, taken using an optical profilometer. The random roughness is noticeable with various peaks and valleys across the surface.

## 6 Test Method and Data Reduction

The overall convective heat transfer coefficient for each test coupon was determined by using Eq. (1) and verified using a first law energy balance (Eq. (2)),

$$Q_{net} = h \cdot A_S \cdot \Delta T_{LM} \tag{1}$$

$$Q_{net} = \dot{m} \cdot C_p \cdot (T_o - T_i) \tag{2}$$

The symbol $\Delta T_{LM}$ was the log-mean temperature difference between the flow and the microchannel walls. In Eq. (2), the net convective heat transfer was given by $Q_{net}=Q_H-Q_L$. The justification of using $\Delta T_{LM}$ was based on the assumption that the wall temperature remained constant through the streamwise and spanwise dimensions and was verified using numerical simulations as discussed below.

**Table 2 Coupon roughness properties**

| Coupon | H ($\mu$m) | Manufacturing method | $R_a$ ($\mu$m) | $R_z$ ($\mu$m) |
|---|---|---|---|---|
| Smooth | 508.6 ± 2.6 | Wire-EDM and polished | 0.14 ± 0.06 | 3.2 ± 0.9 |
| A | 505.6 ± 2.6 | Wire-EDM | 2.6 ± 0.2 | 26.2 ± 2.2 |
| B | 525.6 ± 3.2 | Plunge-EDM | 4.4 ± 0.6 | 38.4 ± 6.4 |
| C | 557.8 ± 5.9 | Plunge-EDM | 6.1 ± 1.7 | 46.2 ± 9.6 |

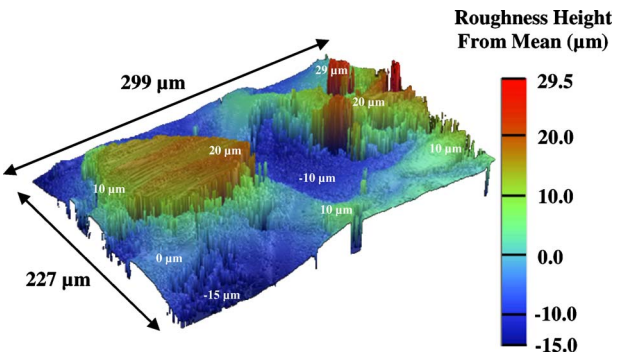


**Fig. 8 Coupon C three-dimensional profilometry surface plot**

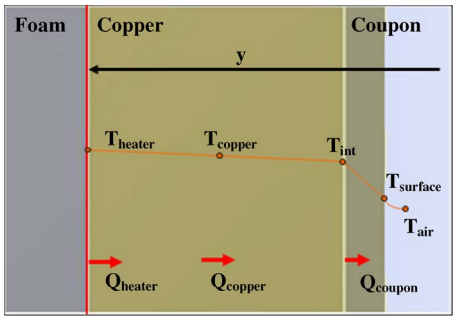


**Fig. 9 Schematic of a cross-sectional view of the test stack (foam to air)**

Due to the small physical size of the microchannels, the internal wall temperature could not be directly measured in this study and was instead modeled using a one-dimensional analysis. The channel wall temperature (Eq. (3)) was calculated using a thermal resistance network from the measured temperature of the copper heat sinks to the channel wall,

$$T_S = T_{CU} - (0.5\Delta y_{CU}) \cdot \left(\frac{Q_{net}}{k_{CU} \cdot A_{CU}}\right) - (\Delta y_C) \cdot \left(\frac{Q_{net}}{k_C \cdot A_C}\right) \tag{3}$$

Between the measured copper temperature and the wall temperature were two thermal resistances from the copper thickness and coupon wall thickness, which is shown in Fig. 9. The temperature drop through the thermally conductive paste was negligible due to the minimal thickness and high conductivity.

To determine the overall friction factor of the microchannels, the density and velocity were defined using channel inlet conditions. In this experiment, $\Delta P$ was defined as the difference in measured total pressures between the upstream and downstream reservoirs and then modified for the sharp expansion loss at the exit, as shown in Eq. (4). For a sharp exit into a large reservoir, the value of K was accepted as 1.0 [14]. By designing a smooth nozzle between the upstream reservoir and the channel inlet, the inlet K value was assumed to be zero. Typical test flow conditions within the microchannels are summarized in Table 3,

$$f = \frac{\left[\Delta P_t - \frac{1}{2}K \cdot \rho_o \cdot V_o^2\right] \cdot D_H}{0.5(\rho_i \cdot V_i^2) \cdot L} \tag{4}$$

## 7 Method Verification and Uncertainty

To determine the validity of the constant wall temperature assumption and resistance network calculation for the channel wall temperature ($T_s$), two-dimensional and three-dimensional steady state heat transfer simulations using the finite element computational software ANSYS 11.0 were performed. These simulations were carried out using the test flow conditions within the smooth coupon stated in Table 4.

The two-dimensional simulation was performed to prove the validity of the one-dimensional resistance network assumption used to calculate $T_s$. This two-dimensional simulation at a streamwise midplane showed good copper temperature agreement with the one-dimensional resistance network.

**Table 3 Typical test flow conditions**

| | |
|---|---|
| Reynolds number, Re | $5\times10^3$–$3.5\times10^4$ |
| $P_i$ (kPa gauge) | 450–620 |
| $T_s$ (°C) | 38–93 |
| $\dot{m}$ (kg/s) | 0.001–0.005 |
| $Q_H$ (W) | 38–110 |

Table 4 Numerical simulation parameters

| | |
|---|---|
| $Q_H$ (W) | 106 |
| Re | $2.4\times10^4$ |
| Nu | 64 |

A three-dimensional simulation was then performed using ANSYS 11.0 fluid link elements to determine the copper spatial temperature variation. The test stand was modeled with the same parameters as the previous two-dimensional simulation. Results indicated that the copper midpoint temperature varied by less than 2°C in the streamwise direction and by less than 1°C in the vertical direction when calculated at the channel midplane. This range was determined to be acceptable given that the overall temperature rise of the fluid was 19–27°C for all tests.

Nondimensional copper heat sink and test coupon temperature contours are shown in Fig. 10. $T_i$ is the air temperature at the channel inlet, and $Q_{net}$ is the net convective heat transfer. This nondimensional temperature is the ratio of the metal temperature rise to the overall air temperature rise through the channel. In addition, the horizontal copper midplane nondimensional temperature is shown in Fig. 11, and the vertical copper and test coupon midplane nondimensional temperatures at the channel inlet, midpoint, and outlet are shown in Fig. 12 for the conditions shown in Table 4. Horizontal and vertical temperature locations are shown in Fig. 10 as a dashed line.

To verify that the heat transfer coefficients were measured accurately, a first law energy was checked as given in Eq. (2). This check used the air temperature rise measured across the microchannel and mass flow rate to calculate the net amount of heat entering the air. The energy balance percentages, which represented the difference between the convective heat transfer measured using Eq. (2) and the convective heat transfer measured using $Q_H-Q_L$, are shown in Fig. 13. For all test coupons, the energy balances match what was expected from the heaters and were within ±8%.

An uncertainty analysis on the friction factor and convective heat transfer coefficient was performed using the partial derivative method described by Kline and McClintock [13]. To calculate the uncertainty of the convective heat transfer coefficient of the channel, 12 parameters were considered: heater individual and total power, channel surface area, copper temperature, copper thickness and test coupon wall height, copper and test coupon thermal conductivity, copper and test coupon cross-sectional area normal to the heaters, and finally the air inlet and outlet temperatures. For a range of Reynolds numbers of $1\times10^4-3.1\times10^4$, the uncertainty varies from 4.1% to 4.3%.

Figure 14 shows the percentage that each parameter contributes to the uncertainty, as a function of the total uncertainty to the convective heat transfer coefficient. The largest contributors to the uncertainty were the microchannel surface area ($A_s$), copper temperature ($T_{cu}$), and outlet air temperature ($T_o$). To reduce this uncertainty, as stated before, multiple temperature measurements were taken at each of the locations. This ensured an accurate average temperature and did not reduce these vital temperature measurements to a single point measurement.

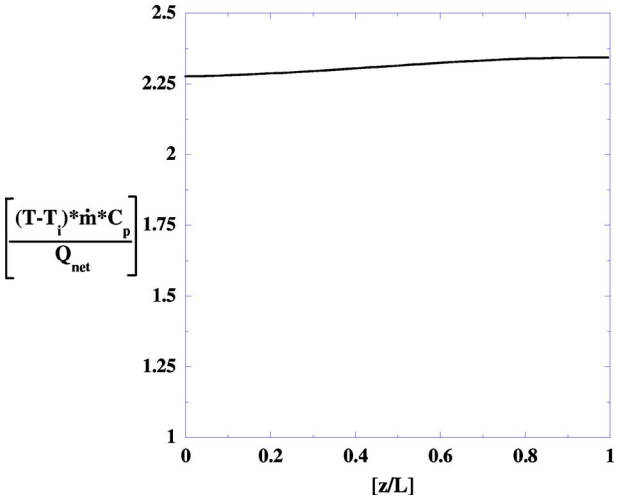


Fig. 11 Copper midplane horizontal temperature distribution

A similar analysis was performed for the friction factor chamber. Figure 15 shows the percentage that each parameter contributes to the uncertainty, as a function of the total uncertainty to friction factor. These parameters were ΔP across the coupon, pressure of the upstream and downstream chambers, air temperature and gas constant, mass flow rate, and the channel height, length, and width. For a range of Reynolds numbers of $8\times10^4-3\times10^4$, the uncertainty varies from 12.3% to 14.3%. Half of this uncertainty came from accurately measuring the channel height. A small 0.01 mm uncertainty in channel height varied the channel area by 2%.

## 8 Heat Transfer Results

Experimental results for heat transfer are shown below in Figs. 16 and 17. Figure 16 also shows two correlations for smooth wall, fully developed, turbulent internal channel flow. These correlations are the Dittus–Boelter correlation [15], as shown in Eq. (5), and the Gnielinski correlation [15] shown in Eq. (6). In the Gnielinski correlation, the friction factor is assumed to be the Blasius smooth wall, fully developed, turbulent internal channel flow correlation [14], as described in Eq. (7),

$$\mathrm{Nu} = 0.023 \cdot \mathrm{Re}^{0.8} \cdot \mathrm{Pr}^{0.4} \tag{5}$$

$$\mathrm{Nu} = \frac{\left(\frac{f}{8}\right)\cdot(\mathrm{Re}-1000)\cdot\mathrm{Pr}}{1+12.7\left(\frac{f}{8}\right)^{0.5}(\mathrm{Pr}^{2/3}-1)} \tag{6}$$

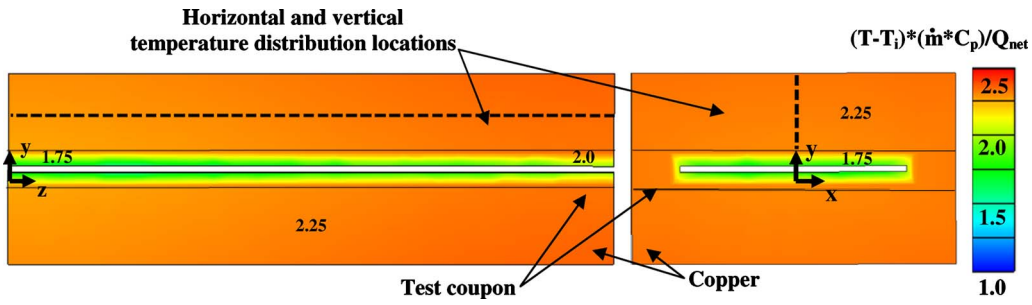


Fig. 10 Three-dimensional ansys simulation of copper heat sinks and test coupon temperatures

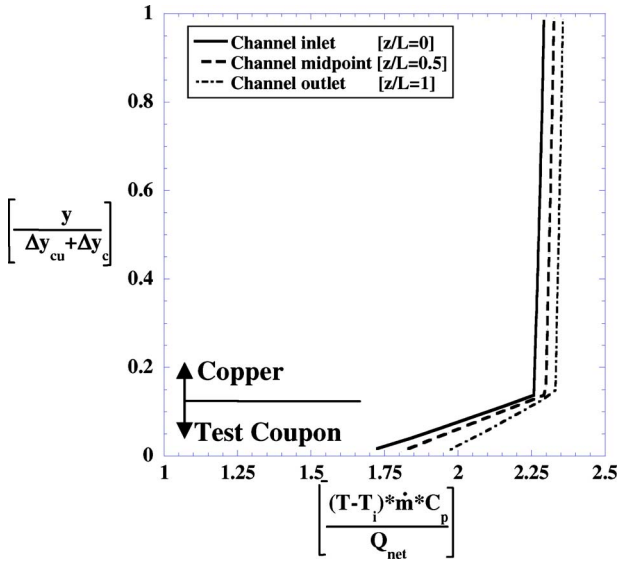


**Fig. 12 Copper and test coupon midplane vertical temperature distribution**

$$f = 0.316 \cdot Re^{-0.25} \quad (7)$$

Figure 17 shows the heat transfer augmentation for the four coupons with the Dittus–Boelter correlation used as the assumed smooth wall heat transfer Nusselt number. Within uncertainty, the smooth wall test coupon agreed with the smooth wall Dittus–Boelter correlation, with a percent difference of only ±4% through the range of Re numbers tested. Coupons A and B showed no surface roughness effect on heat transfer, indicating that average roughness levels of $R_a$ of 2.6 $\mu$m and 4.4 $\mu$m had no effect. These two roughness levels translate to 1.0% and 1.7% of the channel height, respectively. Coupon C, with $R_a$=6.1 $\mu$m that is equated to 2.2% of the channel height, indicated a measurable augmentation on the heat transfer coefficient of the microchannel. This roughness augmented the heat transfer coefficient by 1.1–1.2 for Re=$1\times10^4$–$3\times10^4$.

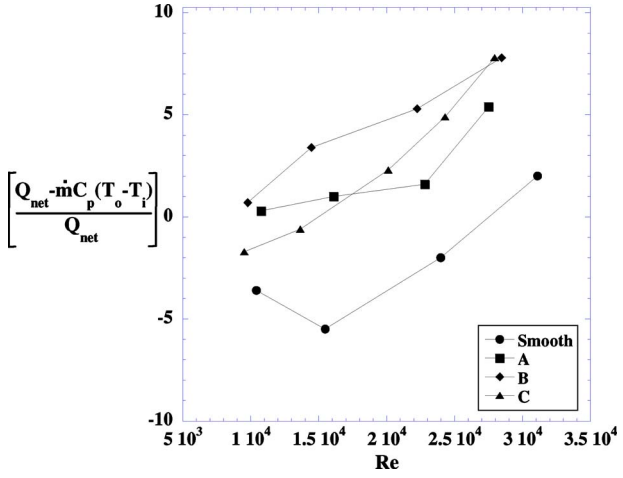


**Fig. 13 Test coupon energy balance percent as a function of Reynolds number**

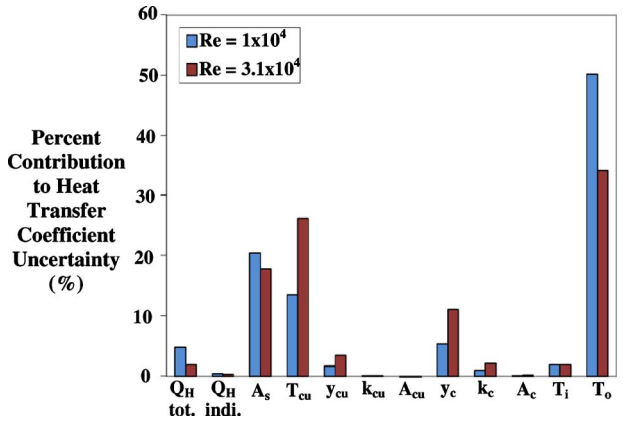


**Fig. 14 Individual parameter contributions to overall heat transfer coefficient uncertainty**

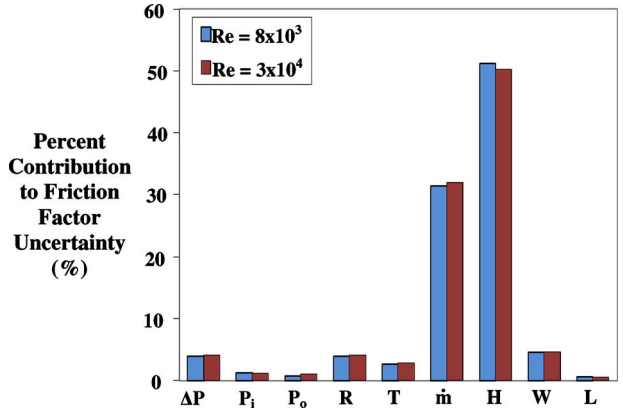


**Fig. 15 Individual parameter contributions to overall friction factor uncertainty**

## 9 Friction Factor Results

Experimental results for friction factor are shown below in Figs. 18 and 19. In Fig. 18, the data are plotted with the Blasius smooth wall correlation, as described in Eq. (7). The smooth wall coupon matched the Blasius correlation well, with a maximum percent difference of 12.3%. As seen in Fig. 19, the three roughened test coupons showed a higher friction factor augmented by 1.8–2.6 over the Blasius smooth wall correlation. Coupon A has a friction factor augmentation of 1.8–2.0, and coupon B has an aug-

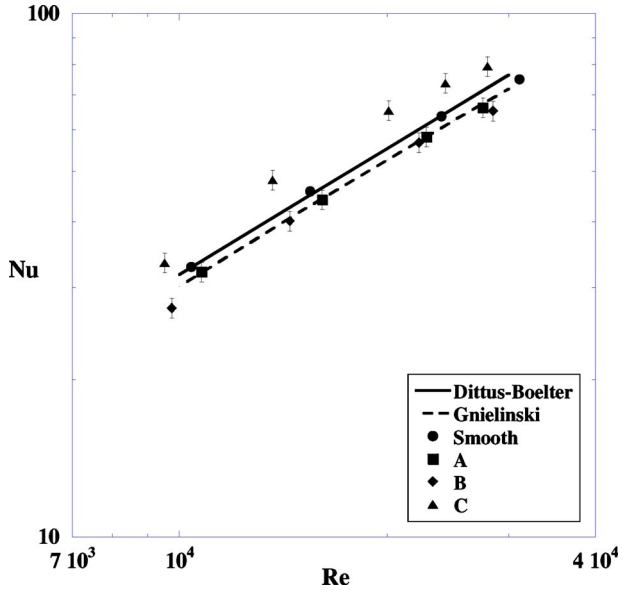


**Fig. 16 Test coupon Nusselt number as a function of Reynolds number**

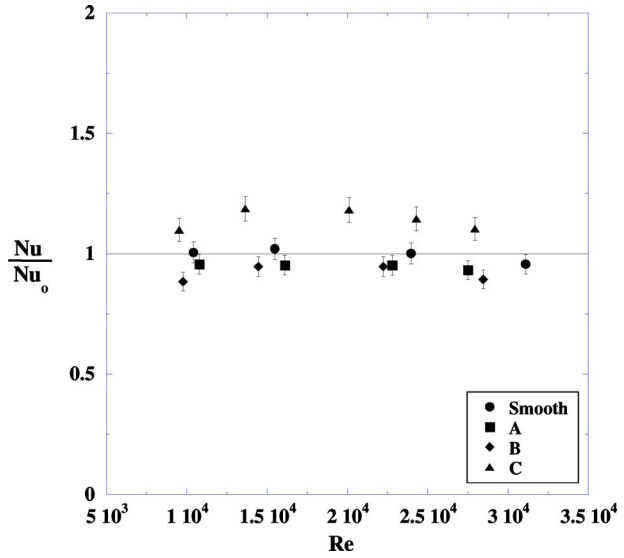


**Fig. 17 Test coupon Nusselt number augmentation as a function of Reynolds number**

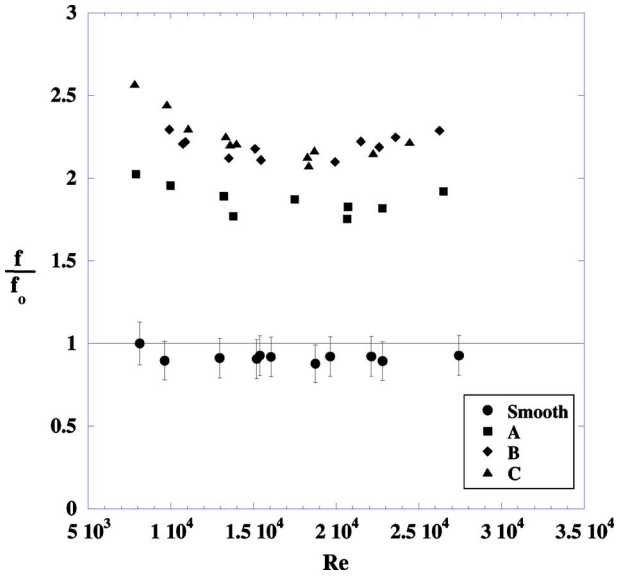


**Fig. 19 Test coupon friction factor augmentation as a function of Reynolds number**

mentation of 2.1–2.3, while having no convective heat transfer increase. Coupon C has a slightly higher friction factor augmentation of 2.1–2.6, but with a discernible convective heat transfer augmentation, as indicated in the previous section.

The augmentations arising from the heat transfer and friction factor results follow the trend of rib turbulated internal channel flows where the pressure drop is generally augmented by a larger amount over a smooth channel than is the heat transfer. These differences in augmentation between pressure drop and heat transfer were demonstrated by Park et al. [16] and Han and Zhang [17]. These differences between augmentation of heat transfer and pressure drop are consistent with the literature and occur as a result of the recirculation regions that occur downstream of the protrusions. These recirculation regions contribute to pressure losses but do not contribute to additional heat transfer augmentation.

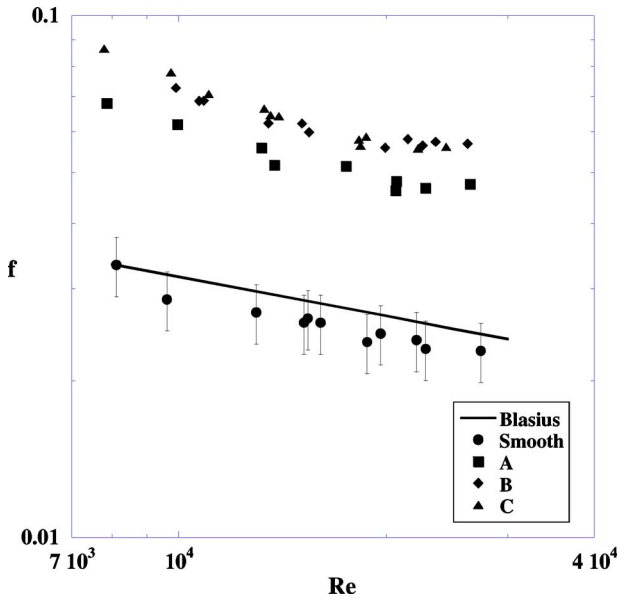


**Fig. 18 Test coupon friction factor as a function of Reynolds number**

## 10 Conclusions

Two test chambers have been developed for quantifying heat transfer coefficients and pressure drops in internal cooling microchannels. At the scale of these channels, the heat transfer and pressure drop can be discernibly affected by the inherent surface roughness due to the manufacturing process. Three roughened channels were manufactured at the level of typical casting techniques, along with a smooth channel to compare with known correlations from the literature. Nusselt numbers and friction factors were reported for the four roughness ratios.

The results for the smooth channel matched the known correlations for Nusselt number and friction factor over the range of Reynolds numbers tested. The channels with $R_a$=2.6 $\mu$m and 4.4 $\mu$m showed no heat transfer augmentation but did show a friction factor augmentation of 1.8–2.3 over the smooth-walled channel. The channel with the highest $R_a$=6.1 $\mu$m showed a heat transfer augmentation of 1.1–1.2 and a friction factor augmentation of 2.1–2.6.

These results indicate that in the range of known casting techniques, the manufacturing surface roughness has an effect on the heat transfer augmentation when the roughness approaches 2.2% of the channel height. Similar to rib turbulated channels, however, the manufacturing roughness had a much larger impact on the increased pressure losses than on the heat transfer augmentation.

## Acknowledgment

The authors would like to thank United Technologies Pratt & Whitney for sponsoring this research work, along with their partners and advisors Atul Kohli and Christopher Lehane.

## Nomenclature

A = area
$C_p$ = specific heat
$D_H$ = hydraulic diameter
f = friction factor: $f=(\Delta P/0.5(\rho_i \cdot V_i^2)) \cdot (D_H/L)$
h = heat transfer coefficient
H = microchannel height
k = thermal conductivity
K = loss coefficient
L = channel length
$\dot{m}$ = mass flow rate
Nu = Nusselt number: $Nu=h \cdot D_H/k_{air}$

$P$ = pressure
$\Delta P$ = pressure difference
$\Delta P_t$ = total pressure difference
$Q_H$ = power from heaters
$Q_L$ = energy loss
$Q_{net}$ = net convective heat transfer
$R$ = gas constant
$R_a$ = average surface roughness
$R_z$ = maximum surface roughness
Re = Reynolds number: $Re = \rho \cdot V \cdot D_H / \mu$
$\Delta T_{LM}$ = log-mean temperature difference: $\Delta T_{LM} = [(T_S - T_o) - (T_S - T_i)] / \ln((T_S - T_o)/(T_S - T_i))$
$T$ = temperature
$V$ = velocity
$W$ = channel width
$x$ = transverse distance from channel center
$y$ = vertical distance from channel center
$z$ = horizontal distance from channel inlet

**Greek**

$\rho$ = density
$\mu$ = dynamic viscosity

**Subscripts**

c = test coupon
Cu = copper
i = inlet
int = copper and test coupon interface
o = outlet
s = surface

## References


[1] Bunker, R. S., 2008, "The Effects of Manufacturing Tolerances on Gas Turbine Cooling," ASME Paper No. GT2008-50124.
[2] Avallone, E. A., and Baumeister, T., 1996, *Marks' Standard Handbook for Mechanical Engineers*, 10th ed., McGraw-Hill Professional, New York, pp. 13–72.
[3] Saini, R. P., and Saini, J. S., 1997, "Heat Transfer and Friction Factor Correlations for Artificially Roughened Ducts With Expanded Metal Mesh as Roughness Element," Int. J. Heat Mass Transfer, **40**, pp. 973–986.
[4] Chang, W. C., Liou, T., and Lu, M. H., 2005, "Heat Transfer of Rectangular Narrow Channel With Two Opposite Scale-Roughened Walls," Int. J. Heat Mass Transfer, **48**, pp. 3921–3931.
[5] Caney, N., Marty, P., and Bigot, J., 2007, "Friction Losses and Heat Transfer of Single-Phase Flow in a Mini-Channel," Appl. Therm. Eng., **27**, pp. 1715–1721.
[6] Liu, C. W., Gau, C., and Dai, B. T., 2004, "Design and Fabrication Development of a Micro Flow Heated Channel With Measurements of the Inside Micro-Scale Flow and Heat Transfer Process," Biosens. Bioelectron., **20**, pp. 91–101.
[7] Qi, S. L., Zhang, P., Wang, R. Z., and Xu, L. X., 2007, "Single-Phase Pressure Drop and Heat Transfer Characteristics of Turbulent Liquid Nitrogen Flow in Micro-Tubes," Int. J. Heat Mass Transfer, **50**, pp. 1993–2001.
[8] Lorenzini, M., Morini, G. L., and Salvigni, S., 2010, "Laminar, Transitional and Turbulent Friction Factors for Gas Flows in Smooth and Rough Microtubes," Int. J. Therm. Sci., **49**, pp. 248–255.
[9] Marques, C., and Kelly, K. W., 2004, "Fabrication and Performance of a Pin Fin Micro Heat Exchanger," ASME J. Heat Transfer, **126**, pp. 434–444.
[10] Bunker, R. S., Bailey, J. C., Lee, C., and Stevens, C. W., 2004, "In-Wall Network (Mesh) Cooling Augmentation of Gas Turbine Airfoils," ASME Paper No. GT2004-54260.
[11] Bunker, R. S., 2009, "A Study of Mesh-Fed Slot Film Cooling," ASME Paper No. GT2009-59338.
[12] van Rij, J. A., Belnap, B. J., and Ligrani, P. M., 2002, "Analysis and Experiments on Three-Dimensional, Irregular Surface Roughness," ASME J. Fluids Eng., **124**, pp. 671–677.
[13] Kline, S. J., and McClintock, F. A., 1953, "Describing Uncertainties in Single-Sample Experiments," Mech. Eng., **75**, pp. 3–8.
[14] White, F. M., 1994, *Fluid Mechanics*, 3rd ed., McGraw-Hill College, New York, pp. 313–340.
[15] Incropera, F. P., and DeWitt, D. P., 2002, *Fundamentals of Heat and Mass Transfer*, 5th ed., Wiley, New York, pp. 466–495.
[16] Park, J. S., Han, J. C., Huang, Y., and Ou, S., 1992, "Heat Transfer Performance Comparisons of Five Different Rectangular Channels With Parallel Angled Ribs," Int. J. Heat Mass Transfer, **35**, pp. 2891–2903.
[17] Han, J. C., and Zhang, Y. M., 1992, "High Performance Heat Transfer Ducts With Parallel Broken and V-Shaped Broken Ribs," Int. J. Heat Mass Transfer, **35**, pp. 513–523.